International Journal of Thermophysics, Vol. 28, No. 5, October 2007 (© 2007)
DOI: 10.1007/s10765-007-0175-1

Thermophysical Characterization of a CuO Thin Deposit[1]

Jean-Luc Battaglia[2,3] and Andrzej Kusiak[2]

CuO thin deposits on a tungsten carbide (consisting of 9% cobalt) substrate are obtained by physical vapor deposition (PVD) at ambient temperature. The longitudinal thermal conductivity as well as the thermal contact resistance at the deposit–substrate interface are investigated. A periodic photothermal experiment based on infrared radiometry is implemented. The amplitude between the periodic heat flux applied on the sample and the average temperature on the heated area are measured over a low frequency range. The method does not require the absolute measurement of these two quantities given that the thermal properties of the substrate are known. Scanning electron microscopy observations show strong anisotropy and columnar structure of the deposits. Moreover, the chemical composition of the films is obtained using the Auger technique. Cobalt diffuses from the substrate toward the deposit during the deposition process. It is demonstrated that the measured thermal conductivity of the CuO layer mainly rests on the microstructure of the layer instead of the roughness of the sample.

KEY WORDS: radiative photothermal experiment; thermal contact resistance; thermal conductivity; thin film.

1. INTRODUCTION

The thermal conductivity measurement of thin solid films in the form of a coating has been treated thoroughly in the literature. Several

[1] Paper presented at the Seventeenth European Conference on Thermophysical Properties, September 5-8, 2005, Bratislava, Slovak Republik.

[2] Laboratoire inter établissement 'TRansferts Ecoulements Fluides Energétique', UMR 8508, Ecole Nationale Supérieure d'Arts et Métiers, Esplanade des Arts et Métiers, Talence Cedex 33405, France.

[3] To whom correspondence should be addressed: E-mail: jean-luc.battaglia@bordeaux.ensam.fr

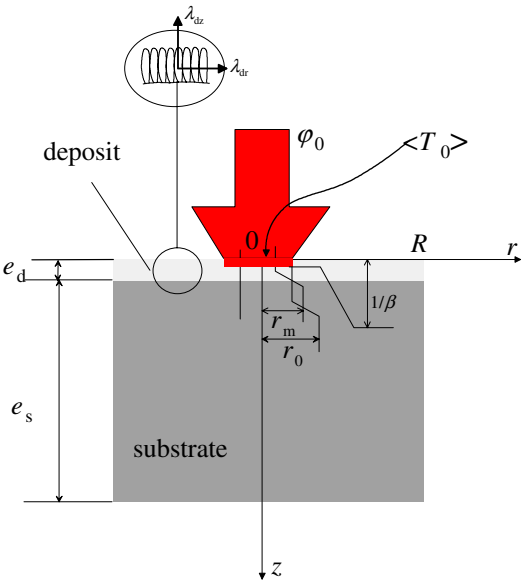

Fig. 1. Deposit thermal characterization using the front face experiment. A transient heat flux density φ is applied on the deposit surface (over a disc of radius r_0), and one measures the average temperature $\langle T_0 \rangle$ on the heated area (over a disc of radius r_m).

experimental approaches are found in the literature based on the front face configuration; see Refs. 1– 7. As represented in Fig. 1, this technique consists of measuring the time-dependent temperature at the location of an incident heat flux applied to the layer. With a periodic heat source, the amplitude and the phase of the response are measured at each frequency. The explored frequency range is defined from the sensitivity of these two quantities according to the thermal properties of the layer. The use of an intermediate approach based on a linear swept frequency heat flux waveform should also be mentioned [5].

This present thermal characterization is only valid for layers whose thickness is more than 10–100 nm, which is the characteristic mean free path of the carriers: phonons and electrons. Below this length, results are not consistent within the meaning of Fourier's law [8,9]. For larger thicknesses, the considerable influence of the deposit–substrate interface on the identified thermal resistance of the deposit is demonstrated. The imperfect contact between the two materials are treated as a thermal contact resistance. As reported in Ref. 10, the influence of the deposition temperature

on the arrangement of the constitutive particles of the layer and on its density is well known. More precisely, particle column-like arrangements are found at a deposition temperature which is far from the melting temperature. In that case, it would be judicious to separately consider a longitudinal and an in-plane thermal conductivity in the layer, which are not comparable with that of the crystal. On the other hand, when the substrate is no longer chemically neutral with respect to the deposit, one must take into account species diffusion phenomena during the deposition process with the deposit–substrate interface. This mass diffusion can have significant effects on the final thermal properties of the layer.

This present work concerns CuO deposits on a WC-Co(9%) substrate. The goal is to explain the measured thermal conductivity of the layer as a function of its microstructure, its chemical composition, and the surface roughness. From Ref. 11, it is shown that the total surface emissivity of the CuO is close to 0.6 in the 0–100°C temperature range. Such a feature improves incident radiation absorption and infrared radiation emission. Therefore, we have used periodic photothermal infrared radiometry in order to estimate the thermal resistance of the CuO layer.

2. FREQUENCY-DOMAIN PHOTOTHERMAL IR RADIOMETRY EXPERIMENT

A schematic view of the experimental setup is shown in Fig. 2. The system is composed of two parts: the thermal excitation and the radiative heat flux measurement. The thermal excitation is generated on the surface of the layer using a laser diode of 808 nm wavelengths and 5 W maximum power. The laser is modulated directly from its driver using a sinusoidal signal from the frequency function generator. Such an external modulation range of the driver is limited to 20 kHz. The laser beam is redirected perpendicular to the surface of the sample and focused by an objective. The laser beam has a uniform profile as specified by the manufacturer. A very fast photodiode is used to measure the reference signal in order to avoid the phase lag due to the laser diode driver at high frequency. The absorption optical thickness in the layer depends on the incident laser beam wavelength. Reference 11 gives $k = 2$ as the extinction coefficient at $\lambda = 800$ nm for CuO. Knowing that the absorbed wave attenuates along the distance z as per $\exp(-4\pi k_\lambda z/\lambda)$, it is found that the optical absorption depth is 32 nm.

Emitted heat radiation from the heated area on the layer is measured using a HgCdTe based photovoltaic infrared detector, cooled to liquid nitrogen temperature (77 K). As reported in Fig. 3, the measurement wavelength range is 5–13 μm. The elliptical mirror coated with highly reflective rhodium (reflectivity 98% in the infrared detector wavelength

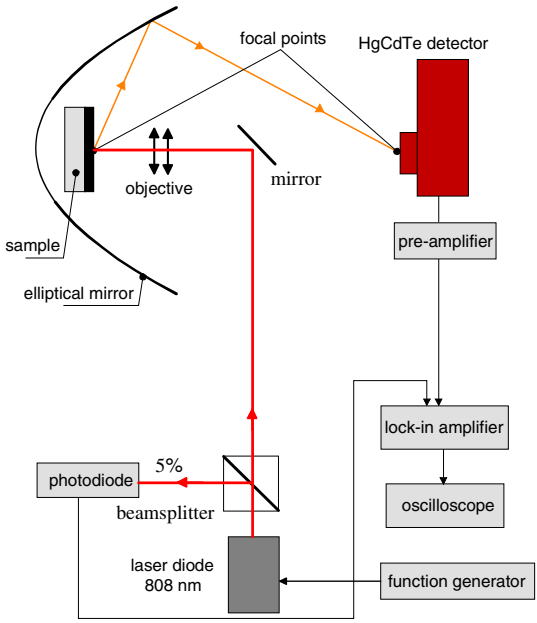

Fig. 2. Schematic description of experimental setup.

band—see Fig. 3) is used to collect the emitted infrared radiation and focus it on the sensor. The heated surface of the sample is located at the interior focal point of the mirror and the sensitive element of the detector at the exterior focal point, which results in a conjugate focused optical system. The incident laser beam is centered and aligned relative to the focal axis of the mirror. The detector wavelength band is well red-shifted with respect to the laser wavelength, which permit the measurement not to be disturbed by the photothermal source. The zone viewed by the detector is the image of the infrared sensitive element on the sample. Given that this element is a square of 1 mm side, the aimed area will correspond approximately to a disk with radius $r_m = 0.5$ mm. The HgCdTe detectivity vanishes when the measured signal frequency is below 10 Hz and it is constant from 10 Hz up to 10 kHz. Therefore, the detector is not sensitive to the dc part of the measured signal.

The signal from the detector is amplified and visualized on a digital oscilloscope together with the photodiode signal. A lock-in amplifier is used to measure the amplitude between the reference and the detector signals as a function of frequency. The signal from the infrared detector is readable up to 2 kHz. As demonstrated later, this value is sufficient to estimate the thermal conductivity of the deposit. The amplitude is only

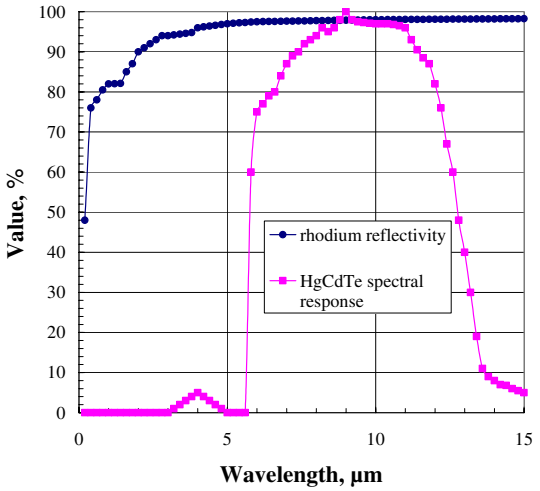

Fig. 3. Spectral response of the infrared detector and the mirror reflectivity as a function of wavelength.

used given that the measurement of the phase is not accurate enough to be used in the estimation procedure. The measurement error concerning the IR detector and the photodiode in the 10–2000 Hz frequency range was studied resulting in constant standard deviations over the entire frequency domain: 0.008 V for the sensor and 0.0075 V for the photodiode. It means that the relative error for the amplitude measurement is less than 5%.

Reference 11 gives a CuO surface emissivity close to 0.5 for $\lambda = 800$ nm but it varies according to the deposition process parameters and to the surface roughness. Thereby, its exact determination involves specific experiments. On the other hand, the incident heat flux cannot be easily quantified even when using the calibration curve from the manufacturer. Thus, the available measurable quantities are the voltages at the HgCdTe sensor and at the photodiode.

In practice, the heat flux comprise of a continuous component which is also called the offset and whose value is at least equal to the magnitude of the sinusoidal component. This offset can be selected large enough in order to increase the detectivity of the sensor but not too much in order to remain in the linear operation range of the detector.

3. HEAT TRANSFER MODEL

We consider low frequency values for the heat flux waveform such that $f << a_d/\pi e_d^2$, where a_d is the thermal diffusivity of the layer and e_d

is its thickness. In that case, the deposit is viewed as a thermal resistance whose intrinsic value is e_d/λ_{dz}, where λ_{dz} is the thermal conductivity of the layer in the z-direction. Thus, according to the geometry represented in Fig. 1, the temperature $T(r, z, t)$ at each point of the medium is a solution of the heat conduction equation in the substrate:

$$\frac{1}{a_s}\frac{\partial T}{\partial t} = \frac{1}{r}\frac{\partial}{\partial r}\left(r\frac{\partial T}{\partial r}\right) + \frac{\partial^2 T}{\partial z^2}, \quad \text{when } 0 < z < e_s, \text{ and } 0 < r < R, \text{ for } t > 0 \tag{1}$$

In this equation, a_s is the thermal diffusivity of the substrate which is assumed to be homogeneous. The boundary conditions at the front surface of the sample involve the heat transfer coefficient h to the ambient and the time-dependent heat flux density φ_0 generated by the laser:

$$T_d - T_s = \begin{cases} R_d\varphi_0(r,t) + hT = \varphi_0 f(r,t) + hT, \\ \quad \text{at } z = 0, \text{ when } 0 < r \leqslant r_0 \\ R_d hT, \quad \text{at } z = 0, \text{ when } r_0 < r < R \end{cases}, \quad \text{for } t > 0 \tag{2}$$

The thermal resistance R_d includes the intrinsic thermal resistance of the deposit as well as the thermal contact resistance R_c at the deposit–substrate interface:

$$R_d = \frac{e_d}{\lambda_{dz}} + R_c \tag{3}$$

The cylindrical symmetry and thermal insulation condition at the periphery lead to the following relation:

$$\frac{\partial T}{\partial r} = 0, \quad \text{at } r = 0, \text{ and } r = R, \text{ when } 0 < z < e_d + e_s, \text{ for } t > 0 \tag{4}$$

The heat transfer at the interface between the rear surface of the substrate and ambient is written as

$$-\lambda_s\frac{\partial T}{\partial z} = hT, \quad \text{at } z = e_d + e_s, \text{ when } 0 < r < R, \text{ for } t > 0 \tag{5}$$

As demonstrated in Ref. 5, applying integral transforms on time and radial coordinates, an expression is found for the following functional form for the average temperature at the surface viewed by the sensor:

$$\langle\theta_m(\omega)\rangle = Z(\omega)\,\varphi_0 \tag{6}$$

In this relation $\omega = 2\pi f$ is the angular frequency, and φ_0 is the amplitude of the periodic heat flux (see Eq. (2)). The transfer function $Z(\omega)$, which corresponds to the spectrum of the impulse response, is found to be

$$Z(\omega) = \frac{r_0^2}{R^2}\frac{\beta_0}{1+h\beta_0} + \sum_{n=1}^{\infty} \frac{4r_0 J_1(\alpha_n r_m) J_1(\alpha_n r_0)}{\alpha_n^2 r_m R^2 J_0(\alpha_n R)^2}\frac{\beta_n}{1+h\beta_n} \tag{7}$$

α_n is the Hankel variable, and

$$\beta_n = \frac{\cosh(k_s e_s) + R_d \lambda_s k_s \sinh(k_s e_s) + h\left(\frac{\sinh(k_s e_s)}{\lambda_s k_s} + R_d \cosh(k_s e_s)\right)}{\lambda_s k_s \sinh(k_s e_s) + h\cosh(k_s e_s)} \tag{8}$$

with

$$k_s = \sqrt{\frac{j\omega}{a_s} + \alpha_n^2} \tag{9}$$

Starting from Eq. (4), approximate values α_n of the radial eigenvalues are found to be

$$\alpha_n R \approx \pi\left(n + \frac{1}{4}\right) - \frac{3}{8\pi\left(n+\frac{1}{4}\right)}, \quad \alpha_0 = 0 \tag{10}$$

The amplitude of the transfer function is finally defined as

$$G(\omega) = 20\log_{10}\|Z(\omega)\| \tag{11}$$

4. SENSITIVITY TO λ_{DZ}

As mentioned in the previous section, the heat flux and the absolute temperature cannot be measured accurately. The measurement of the photodiode and the infrared detector voltage leads to a thermal-wave amplitude, which is controlled by the heat flux, the latter being proportional to the temperature. The sensitivity study for the amplitude evolution versus the frequency and the thermal properties can be used to overcome this drawback. In fact, the lowest frequency behavior of the deposit–substrate system for a large thermal conductivity range is identical to that of the uncoated substrate when the deposit is entirely thermally thin. Such a behavior permits the normalization of the measured amplitude to the theoretical one. From Ref. 12, the known thermal parameters reported in Table I are used to plot the amplitude for different film conductivity values over the frequency interval 1–2000 Hz, as represented in Fig. 4. The

Table I. Thermophysical Properties of the Deposit–Substrate (CuO/WC-Co9%) System

Material	Thickness e_s(mm)	Diameter $2R$(mm)	Density $\rho_s(\mathrm{kg\cdot m^{-3}})$	Thermal conductivity (Hot Disc) $\lambda_s(\mathrm{W\cdot m^{-1}\cdot K^{-1}})$	Specific heat (DSC) $C_{p_s}(\mathrm{J\cdot kg^{-1}\cdot K^{-1}})$
Wc-Co 9%	1 ± 0.01	16 ± 0.01	14264 ± 200	41 ± 4	206 ± 10
CuO	–	–	6300 ± 120	–	460 ± 10

(The thermal conductivity of the substrate was identified using the hot-disk technique [13] and the $(\rho C_p)_d$ product for the deposit was determined by differential scanning calorimetry for C_p and using a volumetric apparatus for ρ using the artificially obtained CuO crystals. These measures are consistent with those found in Ref. 12.)

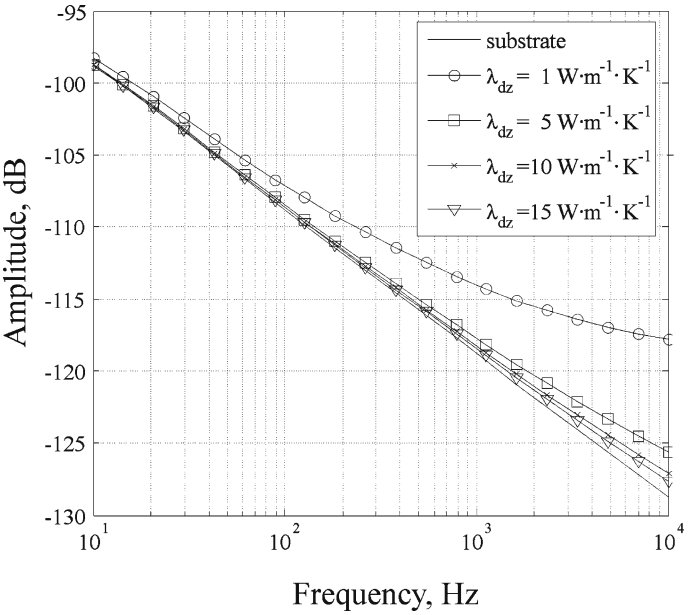

Fig. 4. Sensitivity of amplitude vs. λ_{d_z} in the [10–2000] Hz frequency range. λ_s=41 $\mathrm{W\cdot m^{-1}\cdot K^{-1}}$, $(\rho C_p)_s = 2.938\times10^6\,\mathrm{J\cdot m^{-3}\cdot K^{-1}}$, $e_s = 1$ mm, $e_d = 1\mu$m, $r_0 = 1.5$ mm, $r_m = 0.5$ mm, $h =$ $5\mathrm{W\cdot m^{-2}\cdot K^{-1}}$.

amplitude variation vs. frequency for $10 < f < 2000$ is small but sufficient with regard to the measurement error, thus allowing the estimation of the deposit thermal conductivity.

5. RESULTS

5.1. Deposit Morphology

The WC-Co9% substrate is 16 mm in diameter and 1 mm in thickness. Uniformity of the deposition surface roughness is reached from a high-pressure jet of calibrated Al_2O_3 particles ($\sim 3\,\mu$m diameter). The surface is then cleaned by exposure to ultrasound.

The surface morphology has been measured using an optical interferometer. The probed area is $80\mu\text{m} \times 60\mu\text{m}$ and the measurement has been repeated on three different zones of the surface in order to verify roughness uniformity. The calculated average roughness is $R_a = 300$ nm.

The CuO is deposited using the physical vapor deposition (PVD) technique. Process parameters are RF power density: $1.7\,\text{W}\cdot\text{cm}^{-2}$, substrate temperature: 25°C, deposition rate: $44.8\,\text{nm}\cdot\text{min}^{-1}$, total pressure: 0.5 Pa, oxygen partial pressure: 0.03 Pa (6%), and crystallization state: amorphous. Four samples have been fabricated, with different deposit thicknesses: 0.5, 0.75, 1, and 1.58 μm. The 3D surface morphology has been measured using the optical interferometer for each sample, and roughness average values are reported in Table II. As one can see, the roughness does not vary significantly with the deposit thickness. This result shows that the deposit follows the substrate surface morphology. The film structure has been studied using scanning electron microscopy (SEM). As shown in Fig. 5, the result is a tapered columnar structure with the columns ending in domed tops as suggested in Fig. 1. According to Ref. 10, this observation is consistent with the expected morphology when the value of the temperature deposition is such as $T/T_m < 0.3$, where T_m is the CuO melting temperature. Whatever the deposit thickness, the average grain size is approximately 1 μm and the deposit appears to be clearly anisotropic. In order to measure the chemical composition of each deposit from SEM, a cross-section of each sample was prepared as shown in Fig. 6. Results obtained from retro-diffused electron measurements are reported in Table II. It appears that the CuO composition is homogeneous and independent of the deposit thickness. Nevertheless, a small quantity of cobalt is observed even when the deposit thickness is greater than the

Table II. Roughness Parameter for Substrate Alone and Deposited CuO Layers

	Subtrate alone	$e_d = 0.5\mu$m	$e_d = 0.75\mu$m	$e_d = 1\mu$m	$e_d = 1.58\mu$m
R_a(nm)	302	286	304	300	281
R_t(nm)	3.6	3.1	3.3	2.7	3

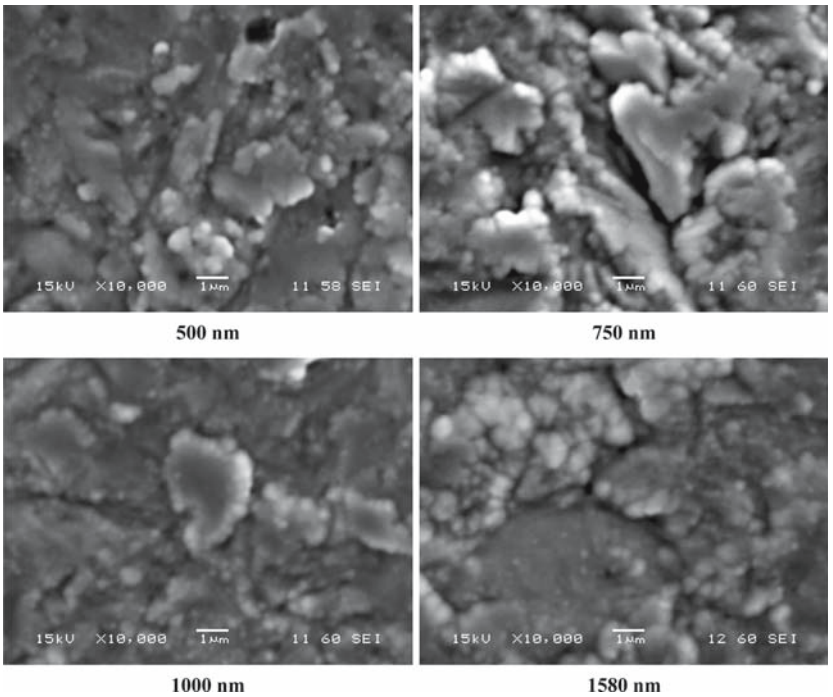

Fig. 5. Deposit structure from scanning electron microscopy.

Table III. Chemical Composition (in mass%) of Sample for 1 μm Depth from the Deposit Surface

	e_d = 500 nm	e_d = 750 nm	e_d = 1000 nm	e_d = 1580 nm
W	6.95 ± 0.56	0.89 ± 0.58		
Co	2.13 ± 0.68	1.10 ± 0.65	0.95 ± 0.57	1.01 ± 0.57
Cu	78.34 ± 1.50	84.97 ± 1.50	84.98 ± 1.32	85.37 ± 1.32
O	12.58 ± 0.10	13.05 ± 0.09	14.07 ± 0.08	13.13 ± 0.08

probed depth. This means that cobalt has diffused into the CuO layer during the deposition process. This result is confirmed from the Auger experiment for which results are presented in Fig. 7.

5.2. Deposit Thermal Conductivity

The periodic photothermal experiments were carried out on the four CuO film samples. The scanned frequency range extents from 10 Hz to

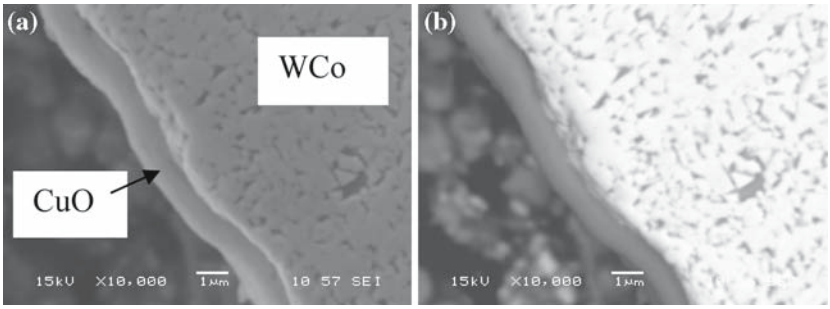

Fig. 6. Cross section of a sample (1 μm thick CuO) observed by SEM in the (a) secondary electron mode and (b) retro-diffused electron mode.

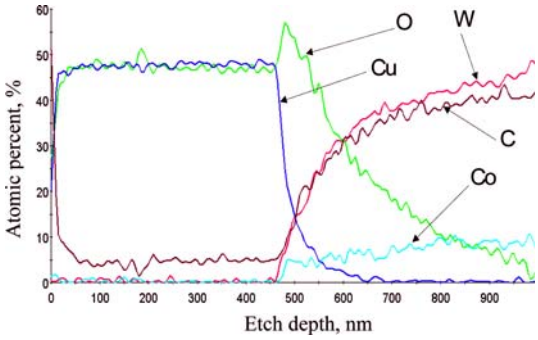

Fig. 7. Chemical composition along z from Auger technique.

2 kHz and was chosen according to the sensitivity analysis presented in Section 4. The heat transfer coefficient with ambient, h, is $5\,\mathrm{W{\cdot}m^{-2}{\cdot}K^{-1}}$. Using the heat transfer model, it is shown that the average temperature on the aimed area is not sensitive to variations of h in the explored frequency range.

The thermal resistance R_d is identified by least-squares minimization between the theoretical and experimental values of $G(\omega)$. The nonlinear least-squares algorithm is described in Refs. 14–15. Figure 8 shows the comparison between the measured and best-fitted amplitudes for each layer. The identified values have been reported in Fig. 9 as a function of the layer thickness.

According to Eq. (3), it is found that, by taking $e_d = 0$ in Fig. 9, the thermal contact resistance at the CuO deposit—(WC-Co) substrate is $R_\mathrm{c} = 4.20 \times 10^{-7} \pm 1.77 \times 10^{-8}\mathrm{m^2 \cdot K \cdot W^{-1}}$ and thus the intrinsic value of the longitudinal thermal conductivity of the CuO is $\lambda_\mathrm{dz} = 3.72 \pm 0.286\,\mathrm{W{\cdot}m^{-1}{\cdot}K^{-1}}$. The in-plane thermal conductivity of the deposit, λ_dr, should differ

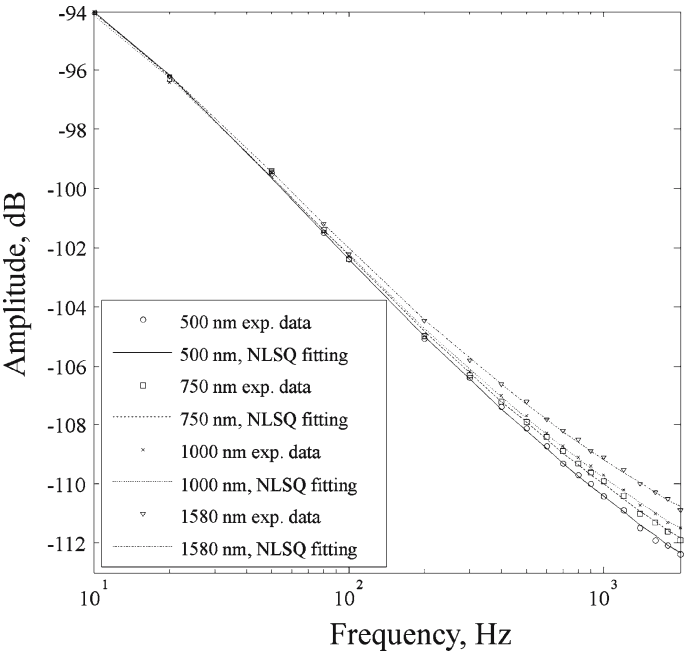

Fig. 8. Measured amplitude and fitted results using a nonlinear least-squares (NLSQ) algorithm for the four CuO layers of different thicknesses. Relative error for the measurement is less than 5%.

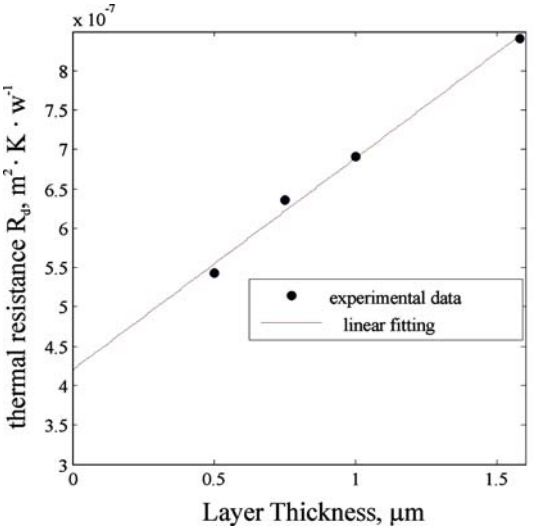

Fig. 9. Identified thermal resistance R_d as a function of the CuO layer thickness.

significantly from the longitudinal value, λ_{dz}, given the anisotropy of the layer represented in Fig. 5. Nevertheless, using the anisotropic model presented in the appendix of Ref. 5, it is shown that the measured quantity $G(\omega)$ is only sensitive to λ_{dr} variation for very high frequencies that are not reached during the experiment.

6. DISCUSSION

A first important result is that the measured roughness and chemical composition are found to be the same for all the samples. The roughness uniformity comes from preparation of the surface using a high-pressure jet of calibrated Al_2O_3 particles of $l \approx 3\mu$m diameter. It is shown that the roughness does not change after the deposition process, which means that the coating follows the surface morphology of the substrate. In the heat transfer model, a perfectly flat surface is assumed and it is thus reasonable to check the validity of such an assumption with respect to ellipsometric measurements. Starting from SEM on the deposit profile represented in Fig. 6, it is observed that the characteristic length for separating roughness is approximately equal to $(l - R_a)\tan\left[\cos^{-1}((l - R_a)/l)\right]$ ($\sim 1.3\,\mu$m assuming a sinusoidal profile for the roughness). This dimension remains large compared to the average roughness value R_a (~ 300 nm). It is thus reasonable to consider that heat transfer in the neighborhood of the deposit remains one-dimensional.

Furthermore, the maximum frequency reached during the experiments (2000 Hz) is not sufficiently high to explain a dependence of the measured amplitude on roughness (see Refs. 16 and 17). That means that amplitude behavior, reported in Fig. 8, is only related to the change of the CuO layer thickness for each sample. As expected, a linear variation of the identified thermal resistance R_d is observed dependent on the thickness of the deposit. From this trend, the longitudinal thermal conductivity of the CuO: $\lambda_{dz} \approx 3.84\,W \cdot m^{-1} \cdot K^{-1}$ is obtained, whereas Ref. 18 gives $17\,W \cdot m^{-1} \cdot K^{-1}$ for the crystal. Such a discrepancy is explained from SEM measurements which report a columnar arrangement in the layer (see Fig. 5). Each column ending in domed tops acts as a directionally restrictive heat flux resistance along the axial coordinate (z). Thus, in order to precisely describe heat transfer in the deposit and at the deposit–substrate interface, Eq. (3) must be rewritten in the following form:

$$R_d = \frac{e_d}{\lambda_{dz}} + R_\varphi(e_d) + R_c \tag{12}$$

In this relation, $R_\varphi(e_d)$ denotes the directional resistance that increases with the layer thickness.

The Auger and SEM analysis revealed significant cobalt diffusion (~10%) in the CuO layer. Given that the thermal conductivity of cobalt is $100\,\mathrm{W \cdot m^{-1} \cdot K^{-1}}$, it contributes to a decrease in the thermal contact resistance at the CuO–(WC-Co) interface. Obviously, cobalt diffusion should also have an influence on the thermal conductivity of the CuO layer.

7. CONCLUSION

This study provides an estimation of the longitudinal thermal conductivity λ_{dz} of a CuO deposit on a WC-Co(9%) substrate as well as the thermal contact resistance R_c at the interface between these two materials. Results are obtained using a modulated photothermal infrared radiometry experiment. An analytical solution for the heat transfer model has been found applying the integral transform technique and an optimum modulation frequency range was defined from a sensitivity study. For this frequency range, the deposit is viewed as a thermal resistance that takes into account the longitudinal thermal conductivity of the deposit as well as the thermal resistance at the deposit–substrate interface. The experiment has been performed using four CuO layers of different thicknesses in order to differentiate between λ_{dz} and R_c.

It has been concluded that the measured amplitude is not sensitive to surface roughness. This is due to the surface preparation of the substrate that allows a controlled roughness as well as operation in the thermally thin regime. On the other hand, it appears clearly that the thermal conductivity of the deposit extensively depends on the microstructure. Columnar configuration occurs when the deposition temperature is far from the melting temperature. Such a microstructure leads to directionally restricted heat flux lines with the degree of restriction increasing with layer thickness. Quantification of this directional thermal resistance involves a more detailed analysis of the microstructure, which will be the subject of further work. Finally, it is shown that the thermal contact resistance at the deposit–substrate interface is greatly dependent on the cobalt mass diffusion that occurs during the deposition process.

REFERENCES

1. D. G. Cahill, A. Bullen, and S.-M.Lee, *High Temp.-High Press*. **32**:134 (2000).
2. S. Orain, Y. Scudeller, and T. Brousse, *Int. J. Therm. Sci.* **39**:537 (2000).
3. S. Dilhaire, S. Grauby, W. Claeys, and J.-C. Batsale, *Microelectr. J.* **35**:811 (2004).
4. O. Faugeroux, B. Claudet, S. Bénet, J. J. Serra, and D. Boisson, *Int. J. Therm. Sci.* **43**:383 (2003).
5. J.-L. Battaglia, A. Kusiak, M. Bamford, and J.-C. Batsale, *Int. J. Therm. Sci.* **45**:1035 (2006).

6. D. M. Bhusari, C. W. Teng, K. H. Chen, S. L. Wie, and L. C. Chen, *Rev. Sci. Instrum.* **68**:4180 (1997).
7. G. Langer, J. Hartmann, and M. Reichling, *Rev. Sci. Instrum.* **68**:1510 (1997).
8. G. Chen, *J. Nanoparticle Res.* **2**:199 (2000).
9. Y. S. Ju and K. E. Goodson, *Appl. Phys. Lett.* **74**:3005 (1999).
10. K. G. Sheppard and S. Nakahara, *Process. Adv. Mat.* **1**:27 (1991).
11. H. Wieder and A. W. Czanderna, *J. Appl. Phys.* **37**:184 (1966).
12. D. R. Lide, ed., *CRC Handbook of Chemistry and Physics*, 87th Ed. (CRC Press, Boca Raton, Florida, 2006).
13. M. Gustavsson, E. Karawacki, and S. E. Gustafsson, *Rev. Sci. Instrum.* **65**:3856 (1994).
14. T. F. Coleman and Y. Li, *SIAM J. Optimiz.* **6**:418 (1996).
15. T. F. Coleman and Y. Li, *Math. Program.* **67**:189 (1994).
16. H. G. Walther, *Appl. Surface Sci.* **193**:156 (2002).
17. L. Nicolaides and A. Mandelis, *J. Appl. Phys.* **90**:1255 (2001).
18. A. L. Edwards, *A Compilation of Thermal Property Data for Computer Heat-Conduction Calculations*, UCRL-50589 (University of California, Lawrence Radiation Laboratory, 1969).